Jaret, S.J., et al., 2023, Extreme isotopic heterogeneity in impact melt rocks: Implications for Martian meteorites: Geology, https://doi.org/10.1130/G50564.1

Jaret et al. Supplement

Supplementary Methods

Methods

For each sampling locality feldspar grains were separated from the same (<10 cm) hand samples. Manicouagan samples were separated using the SelFrag electromagnetic pulse disaggregator at the Lamont Doherty Earth Observatory. Individual grains were hand-picked. 23 of the grains from Manicouagan were the recovered fused beads after argon geochronology (Jaret et al., 2018). Degassing during argon analyses has been shown to not affect Pb isotopes (Hemming and Rasbury, 2000). Plagioclase from the Sudbury norite and the Duluth anorthosite were crushed with a standard agate disc mill and hand-picked.

Pb Isotope Chemistry

Two types of feldspars were measured. The fused beads remaining after $^{40}Ar/^{39}Ar$ dating were dissolved and measured after rinsing with DI water without leaching. Fresh feldspars that had not been fused were rinsed with DI water and then leached in 6N HCl for 30 minutes. The acid was removed, and feldspars were then rinsed with DI water 3 times. Feldspars were then leached with 4N HF for 10 minutes. Acid was removed and grains were rinsed in DI water 3 times. The combined leaches were saved for future analyses. 200 microliters of HF was added and the leached grains were capped and put on a hotplate overnight. Samples were dried down and then redissolved in 50 microliters of 0.7N HBr for ion exchange chemistry to isolate Pb.

Pb Ion-Exchange Colum Chemistry

We used 50 microliter columns of 200 mesh AG1X8 anion exchange resin from Biorad Columns were cleaned with DI water and equilibrated with 0.7N HBr. After samples were loaded, they were washed with 0.45 milliliters of 0.7N HBr in three steps and then eluted with water.

Mass Spectrometry

Pb isotopic analyses were collected using dry plasma mode with a Nu Plasma II Multi Collector ICP-MS in the Facility for Isotope Research and Student Training (FIRST) at Stony Brook University. A Nu Instruments DSN was used for desolvation. A 100 microliter per minute glass nebulizer was used for sample introduction. Signal intensity is 0.4V per ppb. Baselines were taken by deflecting the beam with the electrostatic analyzer for 30 seconds at the beginning of each block. Analyses were 1 block of data, 25 ratios per block, and a 2-second integration time for each ratio. Pb isotopes were collected in faraday cups in static mode with 206 in the axial position. Concentration testes were run to match signals of samples and standards, with samples run at either 0.25 ppb or 0.5 ppb. Samples were bracketed with NIST NBS 981 which was used to make a fractionation correction. Signal intensity and run precision was 1.2 % for 0.25 ppb and 0.5 % for 0.5 ppb. The 0.5% uncertainty is largely the ability to reproduce the standard for these low concentration solutions. Data were plotted using IsoExcel (Ludwig 2004).

Electron Probe Microanalysis

EPMA was conducted at the American Museum of Natural History using a Cameca SX5 Tactis. Non-quantitative electron maps were acquired with a 1 micron bean with 30nA current and 15 kv accelerating voltage. Step size for mapping was 2 microns. Quantitative analyese were standardized using Wakefield diopside, and an internal AMNH anorthite standard.

Diffusion Modeling

Estimating fractional resetting of isotopic anomalies during impact melt sheet cooling

To estimate the extent of isotopic resetting during formation and cooling of impact melt sheets, we model the homogenization of periodic compositional variation (Purdy and Kilkaldy, 1971) of isotopic composition C, differing from mean composition C_m, with wavelength $2l$ and half-amplitude A_0. At time t=0 and position x,

$$C(x,0) = C_m + A_0 \sin\left[\pi \frac{x}{l}\right] \quad (1).$$

After time *t*,

$$C(x,t) = C_m + A_0 \sin\left[\pi \frac{x}{l}\right] \exp\left[\left(\frac{-\pi^2}{l^2}\right)(Dt)\right] \quad (2).$$

where *D* is the self-diffusion rate of the element of interest. Rearranging and combining these equations allows one to define $A(t)$ as the compositional difference at any position at time t relative to the starting compositional difference, so that

$$\frac{A(t)}{A_0} = \exp\left[\left(\frac{-\pi^2}{l^2}\right)(Dt)\right] \quad (3).$$

To derive the curves in Figure 2 of the text, equation 3 is solved for varying lengthscales (half-wavelengths) l of 1, 3, and 10 cm of isotopic heterogeneity, and for values of integrated Dt that depend on the position, and hence cooling history, of each point in the melt sheet. We do not assume constant *Dt* for each position, but instead replace *Dt* with τ', where

$$\tau' \approx \int_0^t D_{eff}(t)dt' \quad (4),$$

and

$$D_{eff}(t) = D(t)\emptyset(t) \quad (5).$$

$D(t)$ is the self-diffusion rate of the element of interest at $T(t)$ and $\phi(t)$ is melt fraction at $T(t)$. Thus, $D_{eff}(t)$ depends on both temperature and melt fraction at each time-step and is determined piece-wise numerically by the thermal model described below.

To determine $D_{eff}(t)$ we model self-diffusion (isotopic equilibration) in an impact melt sheet as a function of temperature, using the self-diffusion kinetics determined by LaTourrette et al. (1992) for Ca (to represent Sr), Nd, and Zr (to represent Hf). We also account for the decrease in effective diffusivity accompanying decreasing liquid fraction as the sheet cools, so for each timestep $D_{eff} = D^*\phi$, where ϕ is melt fraction and is assumed to vary linearly from one to zero over the temperature interval 1200 ot 950 °C, similar to the liquidus-solidus interval for typical basalts.

To derive D_{eff} as a function of *t* for each depth in a melt sheet we model cooling of a 200 m thick melt sheet, the approximate thickness of the Manicouagan melt sheet. For simplicity, we assume an infinite sheet geometry with conductive cooling into an infinite half space on the lower side, and constant zero temperature at the surface (Jaeger, 1968). Thermal diffusivity κ is assumed to be 10^{-6} m^2/s. Because real melt sheets are probably more like short finite cylinders, and hence experience cooling from the sides as well, this assumption results in an overestimate of the cooling time and therefore also overestimates the extent of isotopic homogenization. However, we are not including latent heat effects in the calculation, which would counteract this. We are also ignoring convection, which would act to increase homogenization, at least over lengthscales

of melt migration features, but would also significantly decrease cooling times. Because of the likely counteracting effects of these more complicated affects we contend that a more sophisticated model would not change the basic conclusion that isotopic heterogeneity over 1-3 cm lengthscales is retained in significant portions of the melt sheet, as shown in Figure 2 of the text. This is supported by the fact that the durations of cooling and crystallization (hundreds to thousands of years) are similar to those obtained in more sophisticated models (e.g., Onorato and Uhlmann, 1978).

Modeling isochron array and Pb-Pb isotope resetting

To model the effect of partial resetting on isochron and Pb-Pb isotope arrays, we track the isotopic (e.g., $^{87}Sr/^{86}Sr$, $^{143}Nd/^{144}Nd$, and $^{206}Pb/^{204}Pb$) and parent-daughter (e.g., $^{87}Rb/^{86}Sr$, $^{143}Nd/^{144}Nd$, and $^{238}U/^{204}Pb$) ratios of four aliquots (mineral separates or whole-rocks) formed with identical initial isotopic ratios at 2.7 Ga, aged as closed systems until 215 Ma, then isotopically requilibrated to either 50% or 100% at 215 Ma, and then aged until the present. Isotopic equilibration at 215 Ma is modeled as a shift towards the mean isotopic composition of the aliquots in proportion to the assumed extent of fractional resetting. We assume that aliquots will have the same parent-daughter ratios before and after crystallization (except as modified by radioactive decay of the parent with time), because although our model invokes large-degrees of melting followed by recrystallization after the impact event, there is no significant compositional change over whole rock scales, so a similar phase assemblage is likely to crystallize. This results in rotation of isochron arrays about a mean value for some representative lengthscale, or in the case of Pb-Pb isotope arrays, convergence of compositions towards the mean composition. We recognize that homogenization processes in real melt sheets is likely to be much more complex, and parent-daughter ratios will not necessary remain correlated with isotopic compositions as neatly as assumed here. But as long as isotopic and trace element ratios remain correlated to some degree over the lengthscales of interest (e.g., cm-scale distances, as shown above), this model captures the likely first-order features of isochron resetting during crystallization. As examples, Figures S1-S3 shows the behavior of the Rb/Sr, Sm/Nd and one of the U/Pb isochron arrays, and Figure S4 shows the behavior of the Pb-Pb isotope array (see main text for Pb-Pb behavior including Manicouagan data).

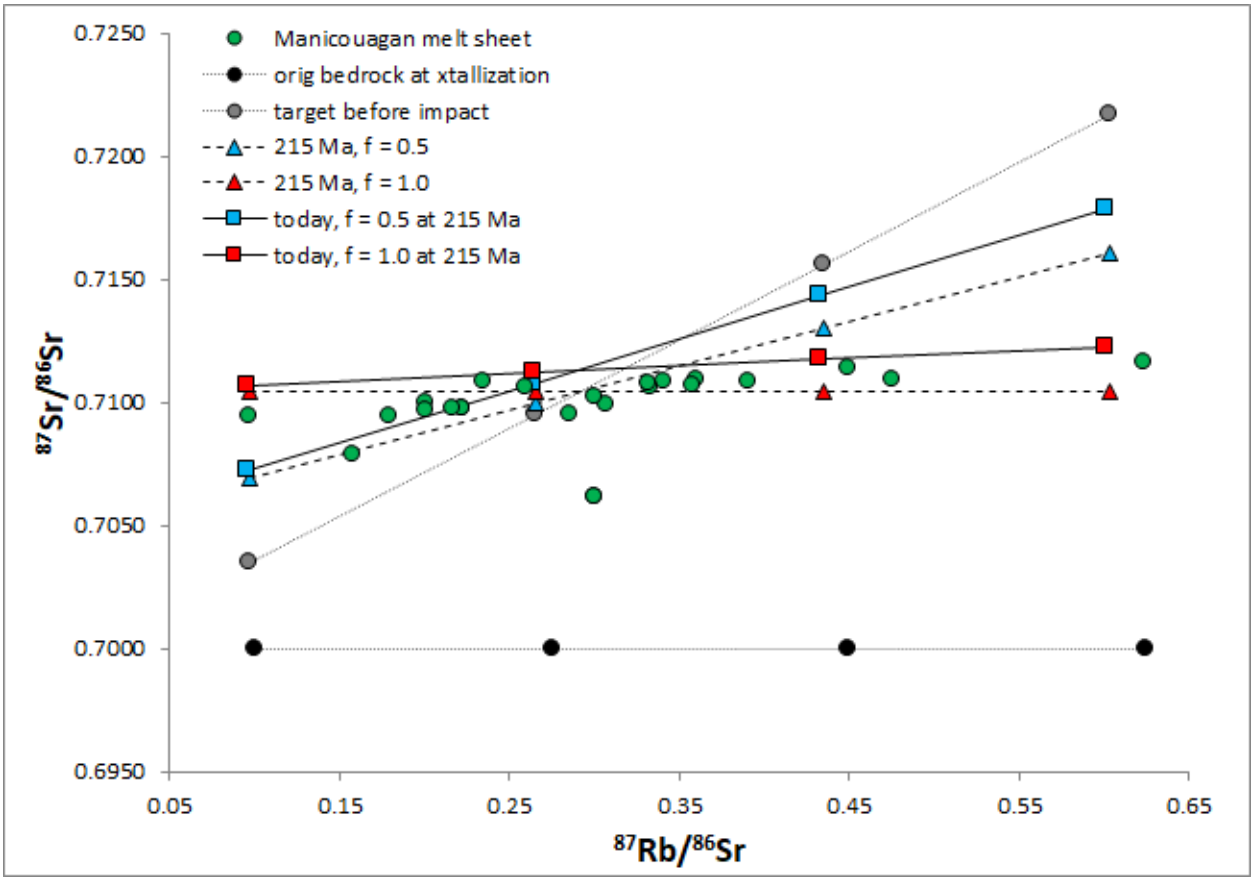

Figure S1. Rb-Sr isochron array at 2.7 Ga (black circles), just prior to impact at 215 Ma (grey circles), just after impact at 215 Ma in the case of full resetting (100% isotopic equilibration) (red triangles) or 50% resetting (blue triangles), and at present for the full resetting (red squares) and 50% resetting (blue squares) cases. The apparent age of the 50% resetting trend (at present) is 1.5 Ga. The age corresponding to the slope of a best-fit line through the Manicouagan melt sheet data is 385 Ma.

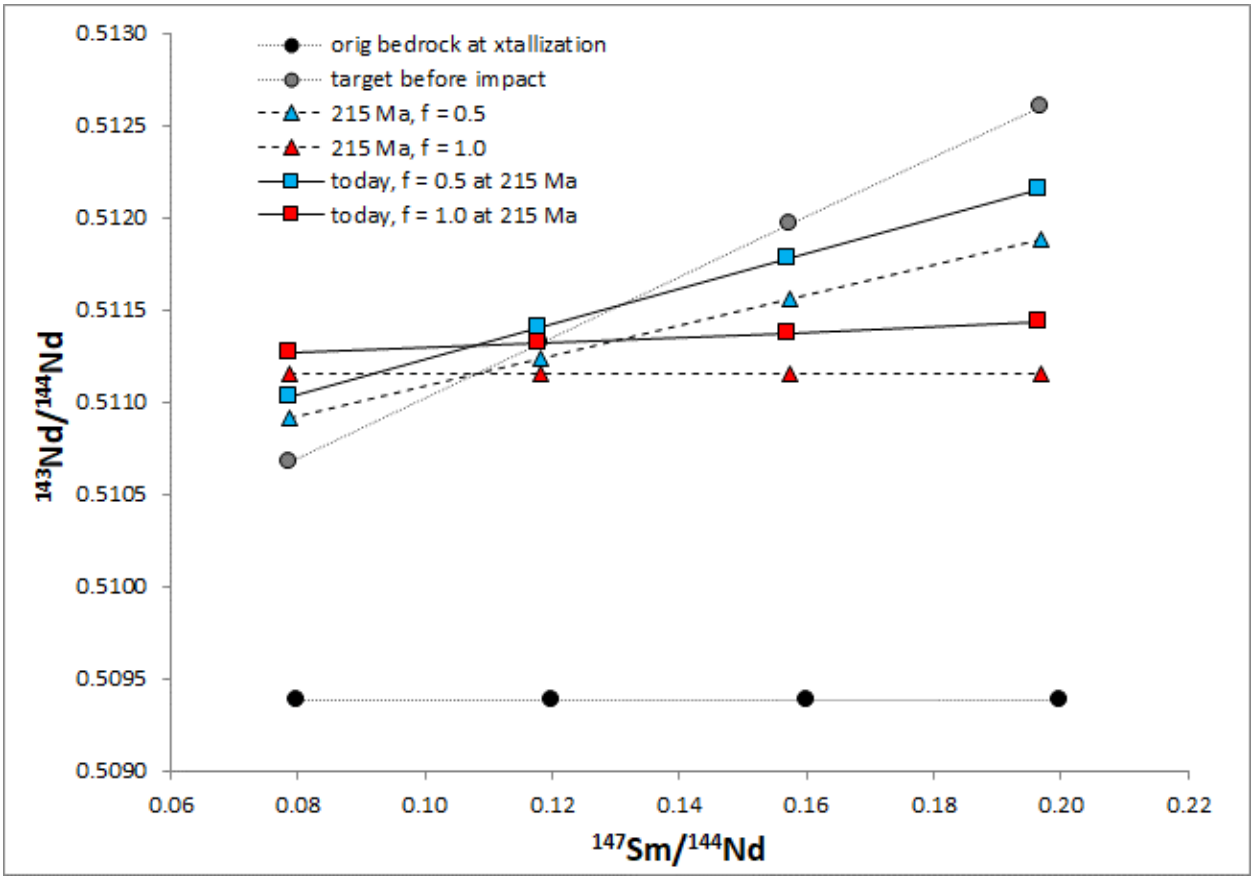

Figure S2. Sm-Nd isochron behavior. Symbols and explanation as in Fig. S1. The apparent age of the 50% resetting trend (at present) is 1.5 Ga.

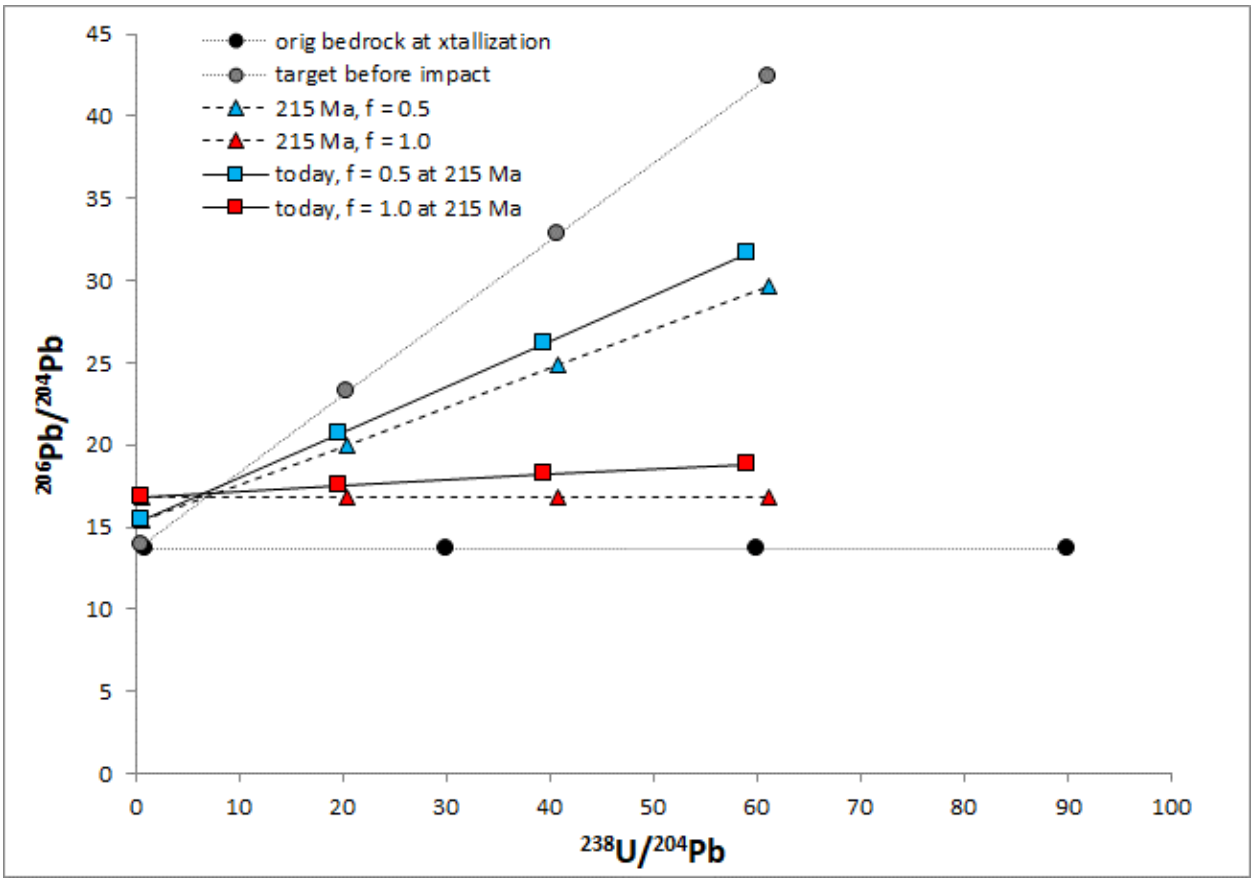

Figure S3. ^{238}U-^{206}Pb isochron array behavior during full and partial resetting. behavior. Symbols and explanation as in Fig. S1. The apparent age of the 50% resetting trend (at present) is 1.6 Ga.

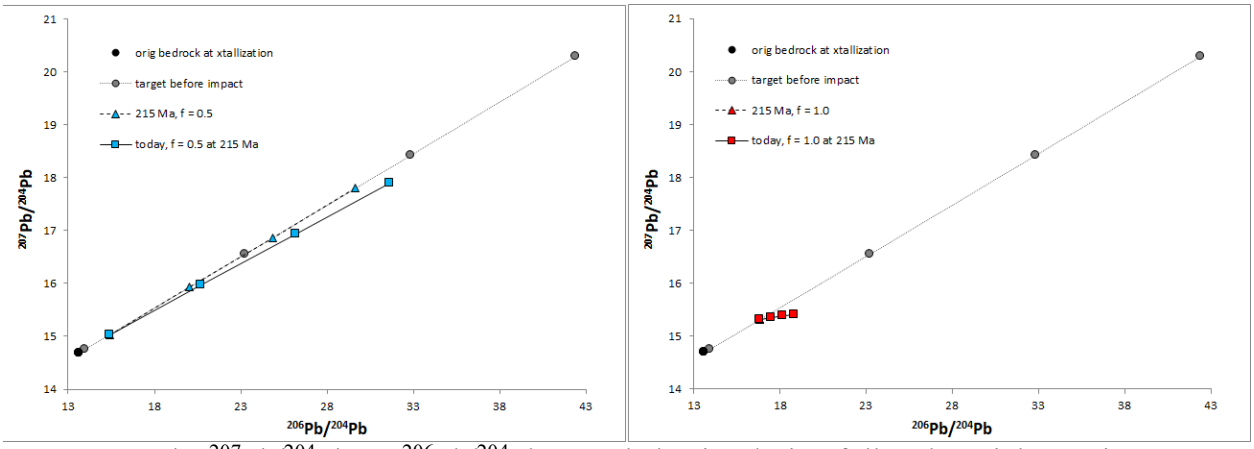

Figure S4. The $^{207}Pb/^{204}Pb$ vs. $^{206}Pb/^{204}Pb$ array behavior during full and partial resetting,

symbols as in Fig. S1. Note that the apparent age of the 50% resetting isochron at present day

(blue text in B) is nearly 2.6 Ga, because incomplete resetting failed to bring all compositions to a single point, as shown in text.

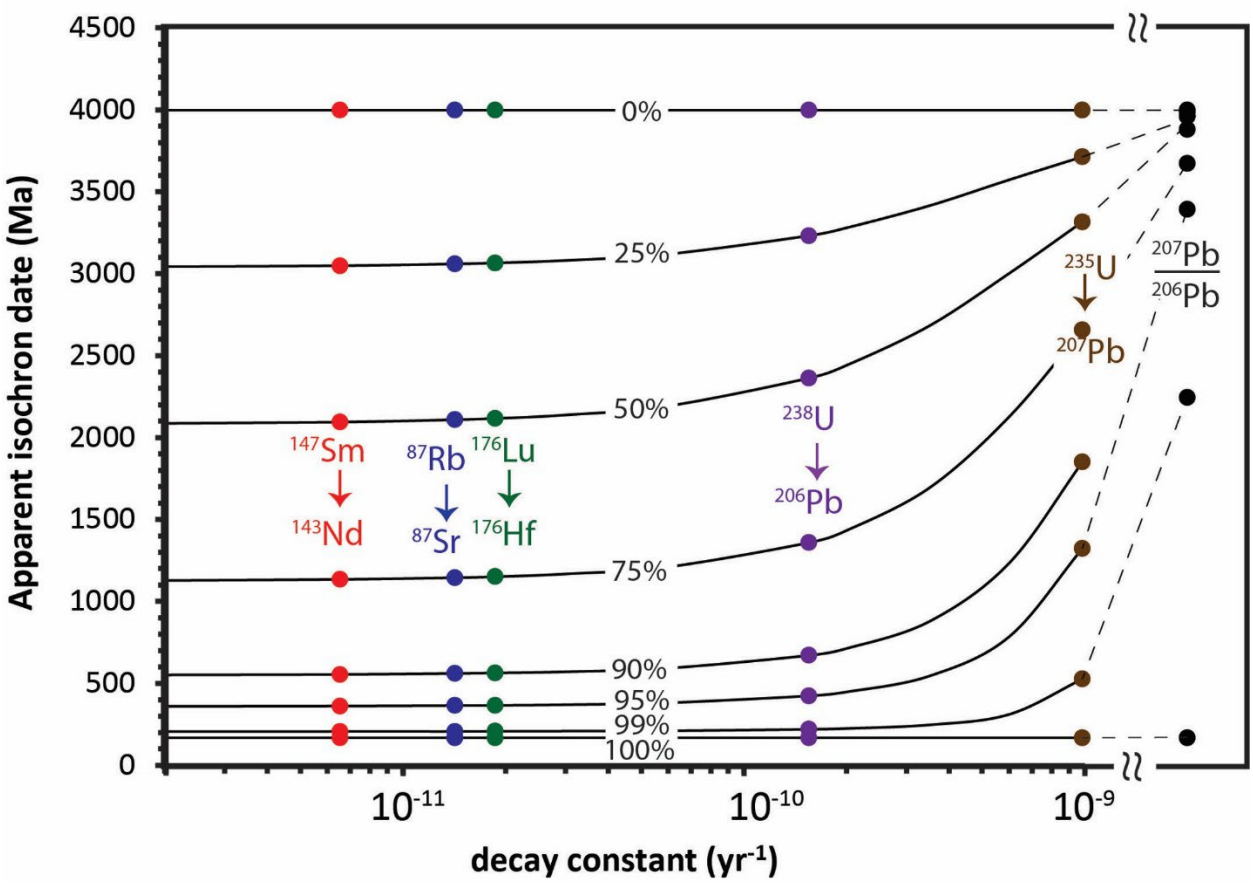

Figure S5. Apparent isochron dates for isochron (and Pb-Pb array) resetting of various extents (percentages shown in black text), assuming an initial isotopic equilibrium (formation) age of 4.0 Ga, impact with resetting at 170 Ma (to simulate one hypothesis for apparent shergottite ages), and continued ingrowth to present (See Supplementary Information). Because of exponential decay/growth with time, systems with larger decay constants result in apparent older dates for a given extent of isochron resetting. The plot is broken before the Pb-Pb isotope array field because this system does not have a single decay constant and results in older apparent dates for another reason as discussed in the text.

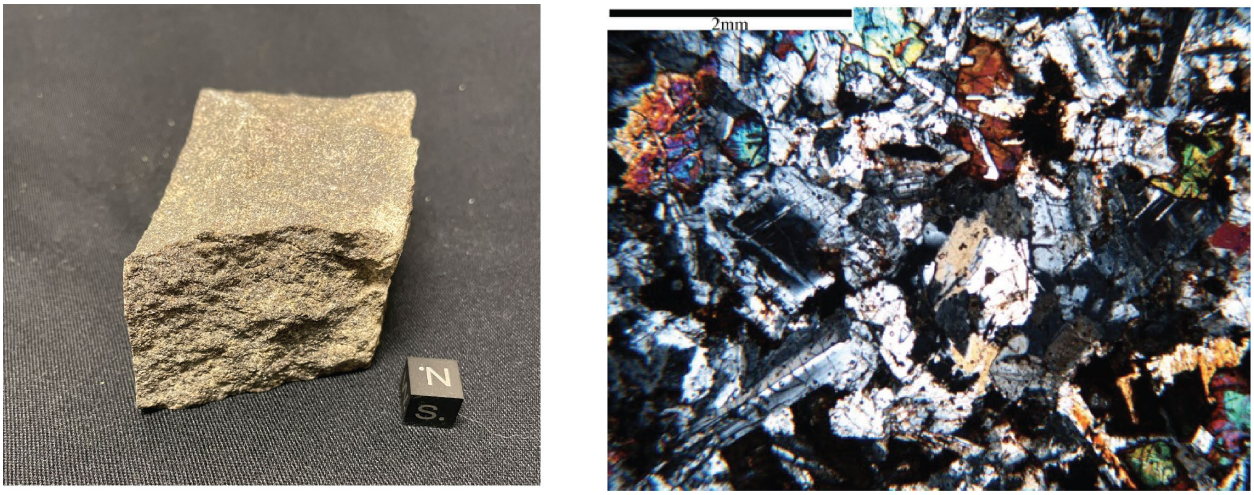

Fig. S6. Hand sample and thin section images of the impact melt rock from the Manicouagan melt sheet at Observation Lake. Scale cube = 1 cm. At both have scales the sample can be seen to have a simple igneous texture with co-occurring quartz, 1-3 mm plagioclase laths, clinopyroxene, and occasional altered amphibole. In some cases, two feldspars are present with plagioclase containing k-feldspar overgrowths. The thin section and the individual feldspar grains analyzed here were taken from the hand sample shown here.

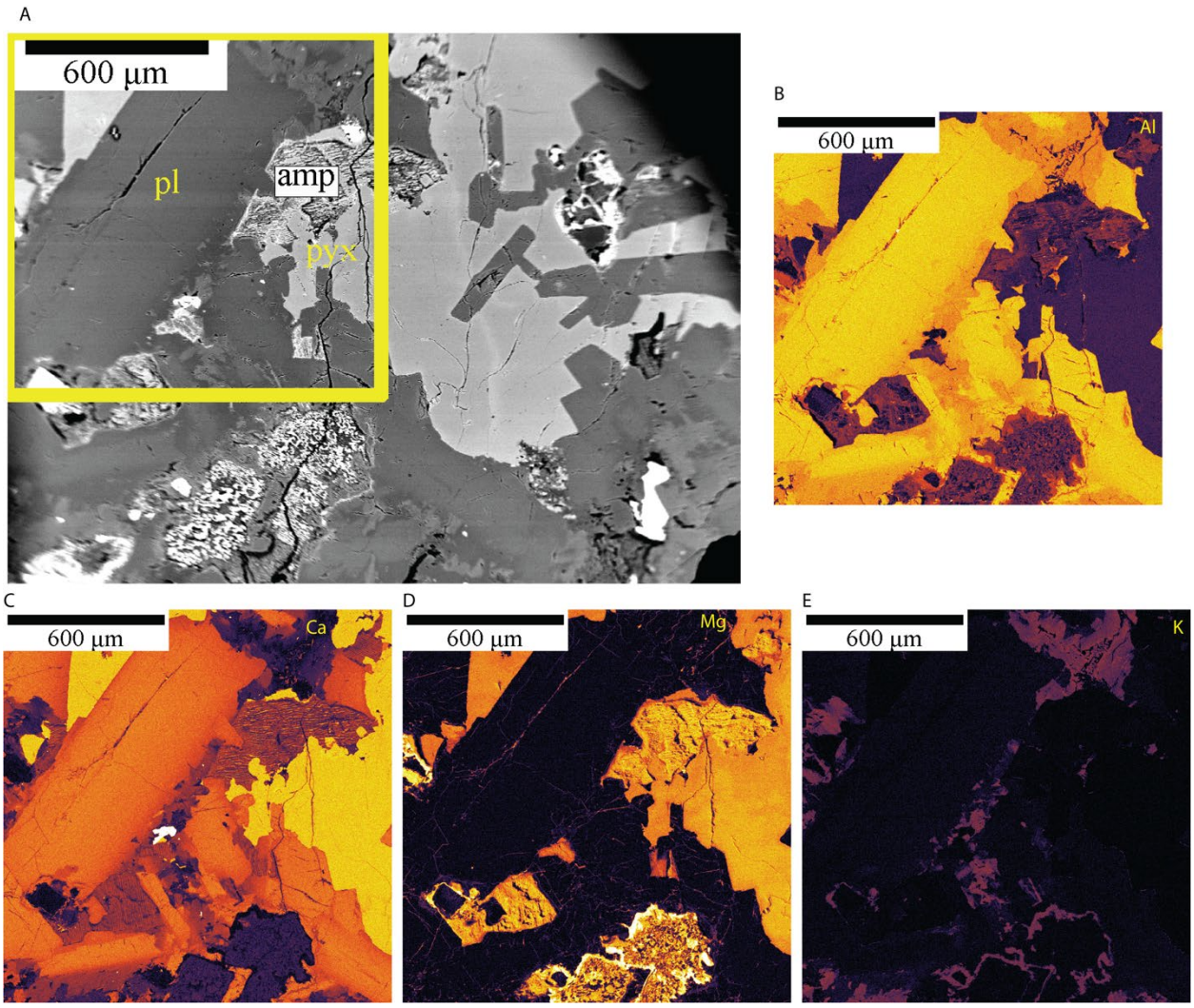

Figure S7: Backscatter Electron image (A) and X-Ray elemental maps for aluminum (B), calcium (C), magnesium (D), and potassium (E) of the impact melt. Plagioclase occur as 1-3 cm laths with minimal zoning and igneous mineral contacts with pyroxene and amphiboles, and minor amounts of quartz.